Iranian Journal of Physics Research, Vol. 23, No. 3, 2023
DOI: 10.47176/ijpr.23.3.11632

Graphitic carbon nitride/MIL-88B(Fe) nanocomposite for methylene blue dye removal from aqueous solution by UV-visible light active photo-Fenton Reaction

S Alijani[1], A Naseri[2*], A Hossein Hamidian[1*]

1. College of Agriculture and Natural Resources, University of Tehran, Karaj, Iran
2. Agricultural Biotechnology Research Institute of Iran (ABRII), Agricultural Research, Education, and Extension Organization (AREEO), Karaj, 3135933151, Iran

E-mail: a.nasseri@abrii.ac.ir

(Received 16 January 2023 ; in final form 24 June 2023)

Abstract

In the present research, g-C_3N_4/MIL-88B(Fe) nanocomposite photocatalyst was successfully synthesized by the solvothermal method. The morphology, crystal structure, chemical functionalities, and optical properties of the obtained nanocomposite were investigated by scanning electron microscopy (SEM), transmission electron microscopy (TEM), X-ray diffraction (XRD), Fourier transform infrared spectroscopy (FTIR), and UV-Vis diffuse reflectance spectroscopy (DRS), respectively. According to the SEM and TEM images, spindle-shaped MIL-88B(Fe) nanostructures were synthesized with an average length and width of 2 and 1 μm, respectively. Furthermore, g-C_3N_4 nanoparticles with an average diameter of 30 nm were observed on the surface of the MIL-88B(Fe). Based on the XRD results, the presence of both g-C_3N_4 and MIL-88B(Fe) nanostructures in the prepared composite was confirmed. Also, the presence of functional groups of the MIL-88B(Fe) and g-C_3N_4 was determined by FTIR. Based on DRS analysis and Tauc's plot, the band gap energy of the prepared composite was measured as 2.1 eV, which indicated that the prepared composite could absorb light in the visible region. The degradation of organic pollutant methylene blue (MB) in the g-C_3N_4/MIL- 88B(Fe)+light+H_2O_2 system was investigated to evaluate the photo-Fenton activity of the prepared composite in comparison with light and light+H_2O_2 systems. The results showed that the presence of g-C_3N_4/MIL-88B(Fe) composite increased the degradation rate of MB pollutant under the photo-Fenton process by 8.1 and 2.8 times higher than the mentioned systems, respectively. Thus, MB removal efficiency reached 100% within 20 min of illumination. The superiority of the g-C_3N_4/MIL-88B(Fe)+light+H_2O_2 system can be attributed to the retardation of electron-hole recombination due to the presence of two nanostructures of g-C_3N_4 and MIL-88B(Fe) in heterojunction, which has led to an increase in the efficiency of the photo-Fenton reaction.

Keywords: environmental remediation, g-C3N4 nanosheets, MIL-88B(Fe), photo-Fenton catalyst, visible-light

1. Introduction

In recent years, climate change, population increase, and then the growth of industries have caused many environmental challenges. The lack of water resources and their quality decrease are among the challenges affecting different regions. Various pollutants from active industries enter water bodies that cause severe environmental and human life problems. Dyes are used by various industries such as textile, paint, plastic, etc. As a known pollutant, colored wastewater has various health and aesthetic effects on the receiving environment [1]. Methylene blue (MB), a well-known and widely used dye in the textile and medical industries, is one of the organic pollutants of interest in water and wastewater treatment research. Various methods such as flocculation, adsorption, oxidation, biodegradation, photocatalytic degradation, and so on have been used to remove dyes from wastewater [2].

The advanced oxidation process (AOP) is an appealing method to remove organic pollutants resistant to biodegradation or as a pre-treatment approach to convert these toxic chemicals into simpler molecules. AOP includes various methods containing photocatalytic oxidation, ozonation, Fenton and pseudo-Fenton processes, etc. AOP is based on the production of free

radicals, the most important of which is the hydroxyl radical [3]. The Fenton process and photocatalyst are preferred among the AOPs used to remove organic pollutants due to their simple application. On the other hand, the Fenton process degrades many organic compounds without producing any dangerous by-products [4]. In the Fenton process, hydrogen peroxide is decomposed by ferrous ions, producing hydroxyl radical. The photo-Fenton process combines UV radiation and Fenton's catalyst to produce free radicals [3,5].

The photocatalytic process has attracted much attention as another method of removing organic pollutants. High efficiency, operation in the presence of cheap, renewable, and abundant energy sources from the sun, and the production of safe by-products make using photocatalysts a priority [6]. Consequently, applying a photo-Fenton reaction in the presence of an effective photocatalyst can improve the efficiency of organic pollutant degradation.

Metal-organic frameworks (MOFs) are a group of porous compounds consisting of organic ligands and metal clusters. High specific surface area and pore volume, adjustable surface properties, stability, and reusability have made them attractive compounds for photocatalytic applications [7]. Iron-based MOFs (i.e. MILs) are porous materials with abundant iron cores, making them excellent Fenton catalysts. Also, the metal nodes of these materials can be directly activated under light irradiation, thus making them more suitable photocatalysts in photo-Fenton systems. Coupling MILs with highly active photocatalysts can increase the rate of organic pollutant degradation due to increasing the rate of free radicals generation.

Graphitic carbon nitride (g-C_3N_4), a metal-free photocatalyst with excellent electronic structure, suitable physical and chemical properties, biocompatibility, and abundance is a promising photocatalyst for environmental remediation [8, 9]. Making heterojunction of g-C_3N_4 with MILs provides a suitable photo-Fenton reagent for removing organic pollutants such as MB [10].

As a result, in the present study, MIL-88B(Fe), an iron-based MOF with promising photocatalytic and Fenton activity [11], was selected in conjunction with g-C_3N_4 nanosheets. Then, g-C_3N_4/MIL-88B(Fe) nanocomposite was prepared and its ability to degrade MB in a photo-Fenton reaction, under UV-Vis. irradiation was evaluated.

2. Experimental section

2.1. Materials

Iron (III) chloride hexahydrate, Dimethylformamide, Terephthalic acid, Glacial acetic acid, Melamine, Hydrogen peroxide 30%, and Methylene blue were purchased from the Sigma-Aldrich company. The materials have been used as received with no more purification.

2.2. Synthesis of g-C_3N_4 nanosheets

To synthesize the g-C_3N_4 bulk structure, 10 g of melamine powder was placed in a semi-closed alumina container and heated at 550°C at a rate of 2.5 °C/min. Then it was kept at this temperature for 4 hours in an insulated furnace. The yellow product (bulk g-C_3N_4) was milled with a mortar to obtain a fine powder. Then, 0.1 g of bulk g-C_3N_4 was added to the mixture of sulfuric acid and nitric acid (20 mL of each acid), and the suspension was stirred for 2 h at room temperature. The resulting white powder was separated from the acid solution by centrifugation and then washed several times with deionized (DI) water to reach pH 7. Then the resulting powder was freeze-dried. Finally, 0.01 g of the white powder was placed in an ultrasonic bath (SONOREX DIGITEC BANDELINE) in 10 mL of DI water at room temperature for 1 h to produce small g-C_3N_4 nanosheets [9].

2.3. Preparation of g-C_3N_4/MIL-88B(Fe) nanocomposite

To prepare this nanocomposite, 1 mg of graphitic carbon nitride powder was first added to 30 mL of DMF solvent and dispersed using an ultrasonic bath for 30 min. Then, while the solution was being stirred in an oil bath at a temperature of 120 °C, 187 mg of $FeCl_3.(H_2O)_6$, 115 mg of terephthalic acid, and 6 µL of acetic acid were added to it. The desired solution was mixed and kept stirring at 120 °C for 210 min to complete the reaction. At the end, the obtained mixture was centrifuged at 12000 rpm and the resulting orange residue was washed with deionized water and ethanol, several times and dried in an oven at 70 °C for 17 h.

2.4. Characterization method

Scanning electron microscope (SEM) and transmission electron microscope (TEM) images, respectively, using FESEM devices; JEOL JSM520 and FETEM; JEOL JEM-2100F were done. AvaSpec2048TEC device was used for diffuse reflectance spectroscopy (DRS). A Perkin Elmer RXI instrument was used to perform Fourier transform infrared (FTIR) spectroscopy. X-ray diffraction (XRD) patterns of the samples were collected on a PANalytical-X'Pert PRO MPD using a CuKα radiation source.

2.5. Photo-Fenton reaction for MB degradation

At first, MB solution with a concentration of 50 mg/L was prepared as a stock solution of the desired pollutant. In each experiment, 50 mL of MB solution with a concentration of 5 mg/L was prepared and used from the stock solution. A UV-VIS spectrophotometer was used to measure the pollutant concentration in the solution. The wavelength was investigated in the 400 to 800 nm range, and the maximum absorption value for MB was determined at the wavelength of 664 nm. To perform the degradation test, 10 mg of g-C_3N_4/MIL-88B(Fe) composite powder and 15 µL of H_2O_2 were added to the MB solution. First, the mixture was placed in the dark for 60 min to perform the adsorption reaction. Then, while air was pumped into the reaction vessel, it was exposed to the radiation of a 15 W UV lamp at a distance of 15 cm from the solution's surface and two 50 W LED lamps at a distance of 9 cm from both sides. Every 10 minutes, 1 mL of pollutant solution was removed from the container and centrifuged for 5 minutes. Then, the concentration of the pollutant remaining in the solution was measured by a spectrophotometer at the desired wavelength and using

Beer–Lambert law. Finally, equation (1) was used to determine the effectiveness of the desired composite in removing the MB pollutant.

$$Removal\ efficiency\ (\%) = \frac{(C_0 - C_t)}{C_0} \times 100, \quad (1)$$

where C_0 is the initial concentration of the pollutant and C_t is the concentration of the pollutant at time t in mg/L.

3. Results and Discussion

3.1. Characterization of g-C_3N_4, MIL-88B(Fe), and g-C_3N_4/MIL-88B(Fe)

The morphology of g-C_3N_4 nanosheets was characterized by TEM. According to figure 1a, g- C_3N_4 nanosheets have a lateral size of about 18 to 40 nm. In the SE micrograph (figure 1b) can be seen that MIL-88B(Fe) nanostructures are spindle-shaped particles with a variable width of 700 nm to 1.5 μm and a length of 1.7 to 2.5 μm. As shown in figure 1c, the g-C_3N_4 nanosheets are well decorated on the MIL-88B(Fe).

Figure 2 shows the FTIR spectra of g-C_3N_4, MIL-88B(Fe), and their nanocomposite in the range of 400-4000 cm^{-1}. For all samples, the broadband in the range of 3000 to 3700 cm^{-1} is vibrations of N-H and/or hydroxyl (O-H) groups on the surface of the samples and/or water adsorbed on the surface. The strong band at 545 cm^{-1} which can be seen for both MIL-88B(Fe) and g-C_3N_4/ MIL-88B(Fe) is attributed to the Fe-O stretching vibration of Fe_3-μ_3- oxo node [10], which confirms the presence of MIL-88B(Fe) inside the nanocomposite. Furthermore, the strong bands at 1390 and 1586 cm^{-1}, seen in the spectra of both MIL-88B(Fe) and nanocomposite are assigned to the C=O symmetric and asymmetric stretching vibration of carboxylate linkers. The broad band in the range of 806-1900 cm^{-1} in the g-C_3N_4 spectrum is attributed to the s-triazine [10].

Some weak bands are observed in this range in the spectrum of the nanocomposite which are assigned to s-triazine due to the presence of g-C_3N_4 in the nanocomposite. As a result, the FTIR spectra confirm the presence of both g-C_3N_4 and MIL-88B(Fe) in the structure of their nanocomposite.

The crystallographic structure of the prepared samples was determined by the X-ray diffraction (XRD) method. As can be seen in figures 3a and b, the prominent diffraction peaks at 2θ of 9 ° and 18 ° of the MIL-88B(Fe) structure are the same in g-C_3N_4/MIL-88B(Fe) nanocomposite. The diffraction peaks at 2θ of 9° and 18° are assigned to the (001) and (101) planes of MIL-88B(Fe), respectively [12]. The ratio of the intensities of (001)/(101) in pure MIL-88B(Fe) was calculated as 1.03, while this ratio was 0.82 for the nanocomposite. This observation confirms the presence of g-C_3N_4 nanosheets beside the MIL-88B(Fe).

Also, a typical peak (001) of interlayer stacking of g-C_3N_4 at 27.9 ° is observed in the XRD pattern of g-C_3N_4/MIL-88B(Fe) nanocomposite, which confirms the presence of g-C_3N_4 inside the nanocomposite structure [13].

Diffuse reflectance spectroscopy (DRS) in the range of visible light wavelength (400-700 nm) for various samples in figure 4a shows the ability of the g-C_3N_4/MIL-88B(Fe) nanocomposite to absorb visible light. As can be seen in figure 4a, g-C_3N_4 nanosheets reflected a large part of the visible light.

The value of the band gap energy for the prepared samples was obtained using the results of DRS analysis (figure 4a), Tauc's plot (figure 4b), and equation (2).

$$(\alpha h\nu)^2 = A(h\nu - E_g), \quad (2)$$

where h is Planck's constant, ν is the frequency of the irradiation photon, α is the absorption coefficient, and A is a constant number. By drawing the curve $(\alpha h\nu)^2$ with the photon energy and linear extrapolation of this diagram, the band gap energy (E_g) for bulk g-C_3N_4, g-C_3N_4 nanosheets, pure MIL- 88B(Fe), and g-C_3N_4/MIL-88B(Fe) nanocomposite, were measured 2.85, 3.0, 2.3, and 2.1 eV, respectively. Therefore, g-C_3N_4/MIL-88B(Fe) nanocomposite has a lower E_g than g-C_3N_4 and MIL-88B(Fe). As a result, it has an excellent ability to absorb light in the visible region and can be a suitable candidate for photo-Fenton activity under sunlight irradiation [14].

3.2 Degradation of MB pollutant by photo-Fenton process

Experiments were conducted to investigate the effectiveness of g-C_3N_4/MIL-88B(Fe) nanocomposite in the degradation of MB pollutant. Since in photo-Fenton reactions, small amounts of pollutants are degraded in the presence of light and/or H_2O_2 without a photocatalyst, control experiments were also performed in different conditions. Figure 5 shows the effect of light and/or H_2O_2 on the removal percentage of MB. As can be seen, when the MB solution, without photocatalyst, was exposed to light along with H_2O_2 (figure 5a), it has the highest percentage of degradation (35.67% in 20 min) compared to the absence of light or H_2O_2.

When the photocatalyst was applied in the photo-Fenton reaction, adsorption was considered in the process (for 20 min) to reach the adsorption-desorption equilibrium. As shown in figure 5b, the removal efficiencies increase significantly in the presence of g-C_3N_4/MIL-88B(Fe). The removal efficiency of MB by g-C_3N_4/MIL-88B(Fe) nanocomposite in the presence of light and H_2O_2 (figure 5b) reached 100% in a short time (only 20 min after the light illumination). It was also observed that the amount of degradation in the presence of light was slightly higher than that of dark condition with H_2O_2.

From the comparison of the results (figure 5c, d), it can be concluded that the presence of g- C_3N_4/MIL-88B(Fe) nanocomposite (figure 5c) causes a significant increase in the degradation efficiency of MB. In figure 5d, the percentage removal of MB under different degradation conditions is plotted. The percentage of degradation was calculated for all conditions from the moment the light source was turned on until 20 min. As can be seen, when the g-C_3N_4/MIL-88B(Fe) nanocomposite was present in the solution, the amount of degradation quickly reached its maximum value (100% in 20 min).

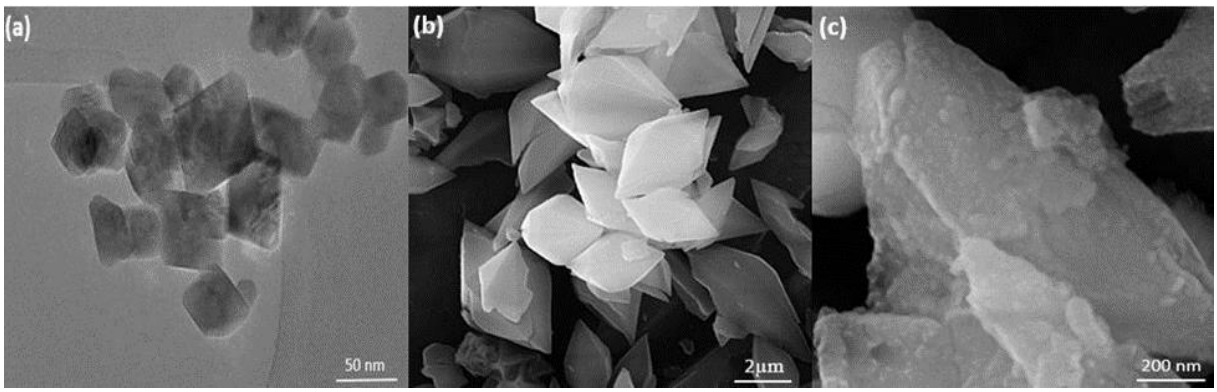

Figure 1. TEM image of (a) g-C_3N_4, SE micrographs of (b) pure MIL-88B(Fe) and (c) g-C_3N_4/MIL-88B(Fe) nanocomposite.

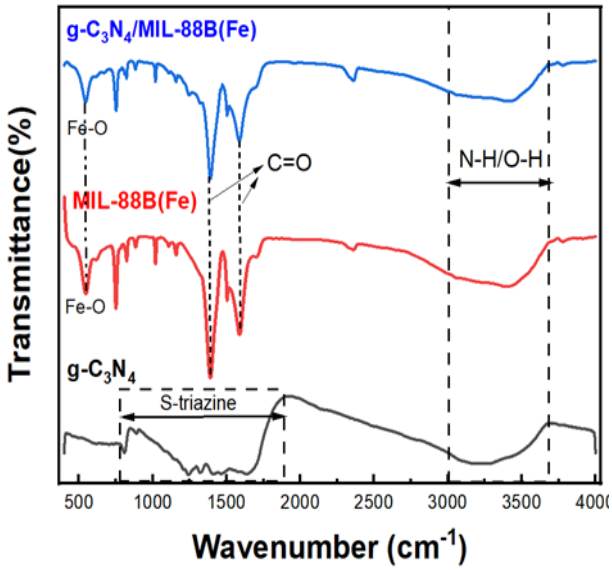

Figure 2. FTIR spectrum of g-C_3N_4, MIL-88B(Fe), and g-C_3N_4/MIL-88B(Fe).

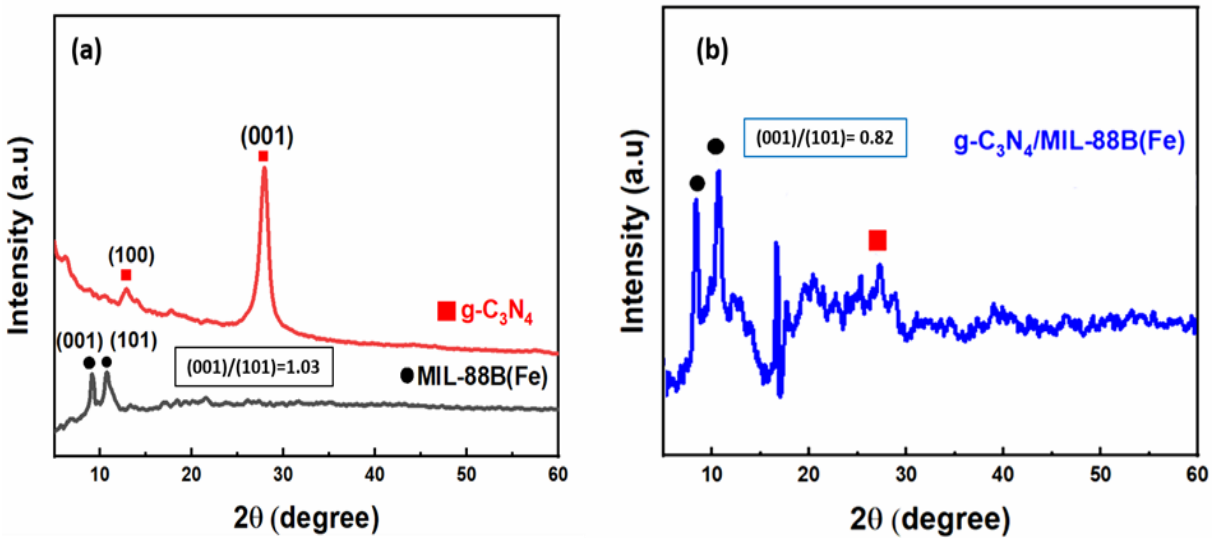

Figure 3. XRD pattern, (a) g-C_3N_4 nanosheets, Metal-Organic framework MIL-88B(Fe), and (b) g-C_3N_4/MIL- 88B(Fe) nanocomposite.

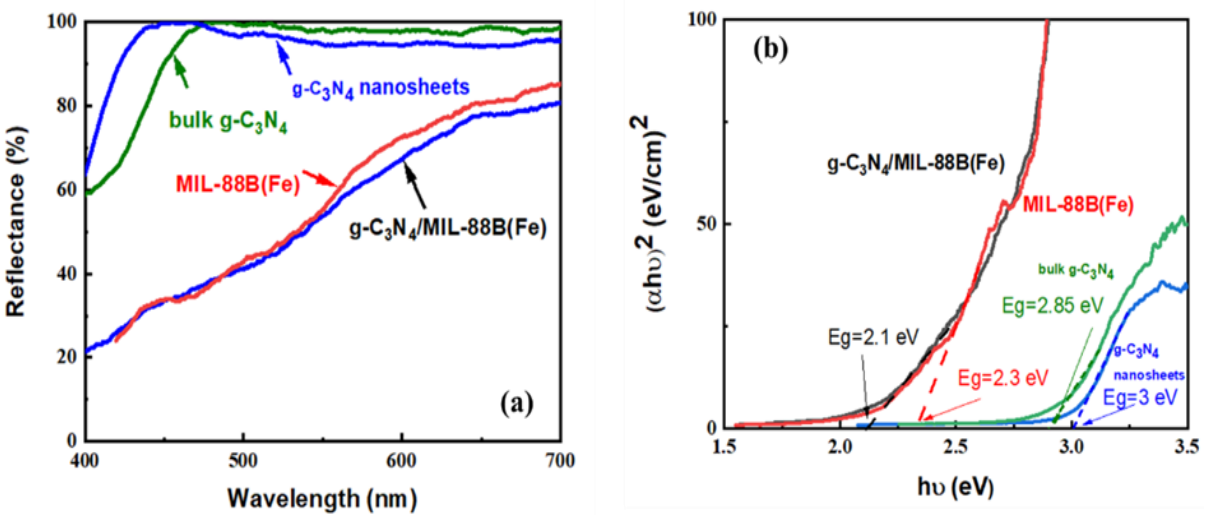

Figure 4. (a) DRS spectra and (b) Tauc's plots of bulk g-C_3N_4, g-C_3N_4 nanosheets, MIL-88B(Fe), and g-C_3N_4/MIL-88B(Fe) nanocomposite, calculated from DRS spectra and Tauc's equation. The extrapolation of the plots' linear ranges show the band gap energies (Eg).

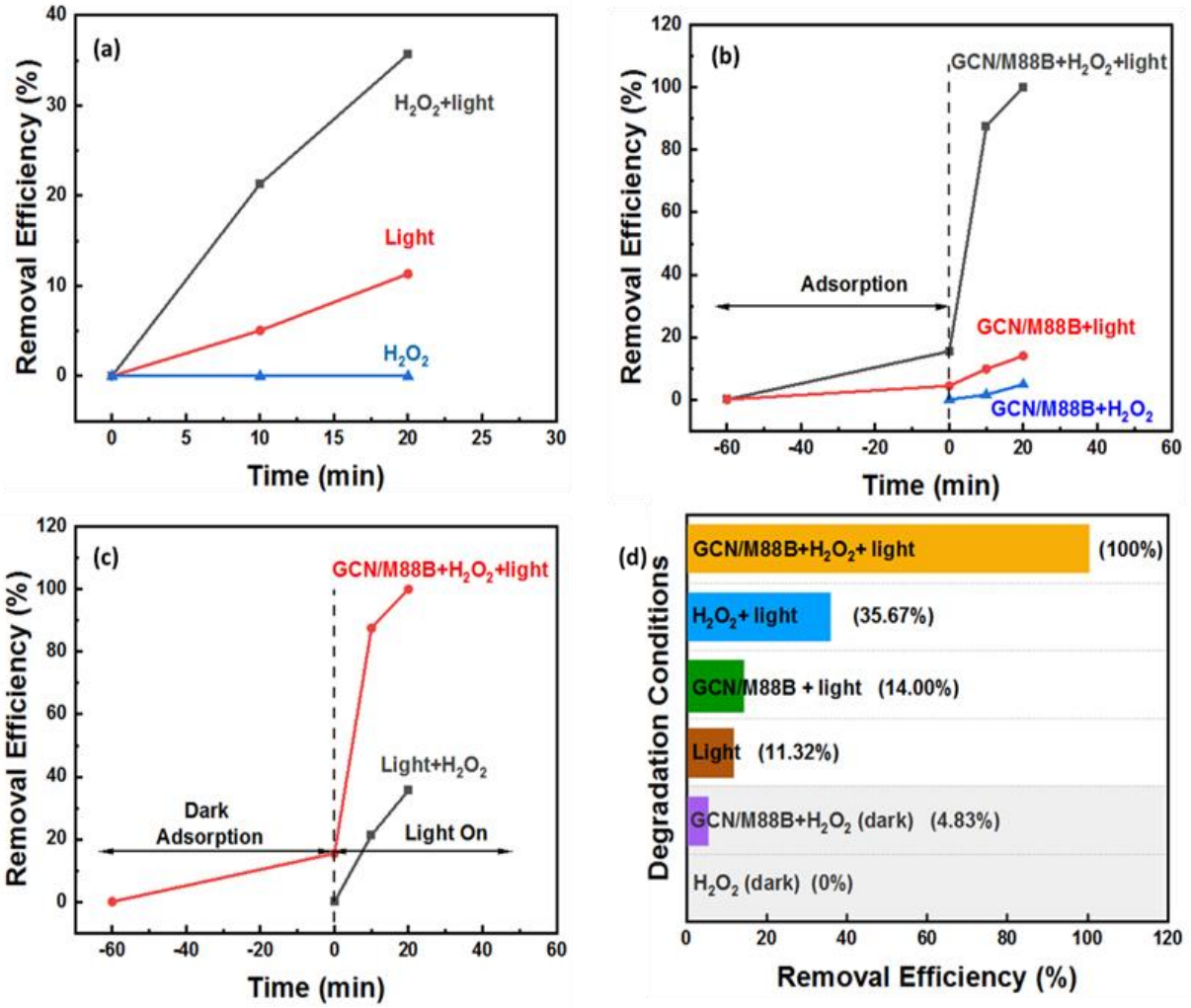

Figure 5. Removal efficiency of MB in the presence of; (a) Light+H_2O_2, Light, and H_2O_2 (in 20 min), (b) g-C_3N_4/MIL-88B(Fe)+H_2O_2+Light, g-C_3N_4/MIL-88B(Fe)+Light, and g-C_3N_4/MIL-88B(Fe)+H_2O_2 (in 20 min), (c) g-C_3N_4/MIL-88B(Fe)+H_2O_2+Light, light+ H_2O_2 (without nanocomposite). (d) Removal efficiencies vs. various degradation reaction conditions in 20 min (a summary of plots, presented in former panels). In all experiments the concentration of MB was 5 mg/L, the amount of H_2O_2 was 15 µL, and the amount of photocatalyst was 10 mg. Also, the applied light source was in the range of UV-Vis.

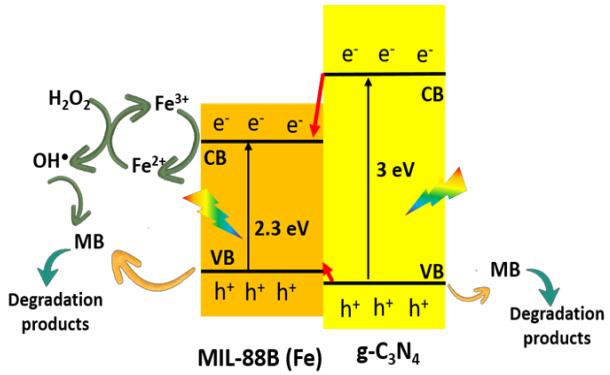

Scheme 1. Proposed mechanism of electron-hole generation, and transfer at the interface of g-C_3N_4 and MIL-88B(Fe) under UV-Vis. light illumination, and the following photo-Fenton reactions at the surface of g-C_3N_4/MIL-88B(Fe) nanocomposite to degrade MB pollutant. ($CB_{MIL\text{-}88B(Fe)}$=-1.55 eV, $VB_{MIL\text{-}88B(Fe)}$=0.73 eV, $CB_{g\text{-}C3N4}$=-2.2 eV, $VB_{g\text{-}C3N4}$=0.8 eV).

To elucidate the effect of the presence of g-C_3N_4/MIL-88B(Fe) nanocomposite on the removal efficiency of MB in a photo-Fenton reaction activated by UV-Vis. light, a mechanism of electron-hole generation, and transfer will be presented. As reported by researchers in previous studies, the valence band (VB) maximum of g-C_3N_4 nanosheets and MIL-88B(Fe) were measured to be located at 0.8 [9] and 0.73 eV [12], respectively. Using the following equation [15] and measured Eg for g-C_3N_4 nanosheets and MIL-88B(Fe) in the section 3.1, the location of the conduction band (CB) minimum of the samples could be calculated;

$$E_{CB} = E_{VB} - E_g\,, \tag{3}$$

As a result, the CB minimum of g-C_3N_4 nanosheets and MIL-88B(Fe) samples are located at -2.2 and -1.55 eV, respectively. Consequently, these two Semiconductors make a type (I) heterojunction, as shown in Scheme 1. As mentioned in equations 4, and 5, under UV-Vis. light illumination, the electron-hole separation occurs in both Fe-MOF (MIL-88B(Fe)) and g-C_3N_4;

$$Fe-MOF + h\nu \rightarrow Fe-MOF(e^- + h^+)\,, \tag{4}$$

$$g-C_3N_4 + h\nu \rightarrow g-C_3N_4(e^- + h^+)\,, \tag{5}$$

As can be seen in Scheme 1, owing to the type (I) alignment of the CB and VB of two semiconductors, the electrons, and holes of the g- C_3N_4 can transfer to the CB and VB of MIL-88B(Fe), respectively. The electrons in the CB of the MIL-88B(Fe) have high reduction potential and can reduce the Fe(III) in the structure of MIL-88B(Fe) to Fe(II) (equation 6). When H_2O_2 is added, the reaction of Fe(II) with H_2O_2 produces a large amount of $OH^\bullet$ (equation 7, 8). Based on the results of other researchers, at first, H_2O_2, as a Lewis base, tends to coordinate with unsaturated iron active sites directly. Then, owing to the existence of extensive Fe-O clusters, Fe-based MIL can be directly excited by light illumination, and the electron-hole pairs are generated immediately. Almost at the same time, photoinduced electrons transfer from O(II) to Fe(III) causing the reduction of Fe(III) to Fe(II). Then, the produced Fe(II) is reacted to the surface coordinated H_2O_2 to start a heterogeneous Fenton reaction, leading to the oxidation of Fe(II) and the generation of hydroxyl radical. In this process, Fe(II) oxidation into its original valence state (Fe(III)) occurs. Therefore, the acceleration of Fe(II)/ Fe(III) cycle is attained upon light illumination, which contributes to increasing the amount of hydroxyl radical and improving the oxidative ability of the whole system [14, 16]. On the other side, the electrons can reduce dissolved O_2 to $O_2^{\bullet-}$ (equation (9)). At last, $OH^\bullet$, $O_2^{\bullet-}$ and holes can degrade MB to less toxic products (equation (10)) [12].

$$Fe^{3+} + e^- \rightarrow Fe^{2+}\,, \tag{6}$$

$$Fe^{2+} + H_2O_2 \rightarrow Fe^{3+} + {}^\bullet OH + OH^-\,, \tag{7}$$

$$Fe^{3+} + H_2O_2 \rightarrow Fe^{2+} + HOO^\bullet + H^+\,, \tag{8}$$

$$O_2 + e^- \rightarrow O_2^{\bullet-}\,, \tag{9}$$

$${}^\bullet OH / O_2^{\bullet-} / h^+ + MB \rightarrow \ldots \rightarrow CO_2 + H_2O\,, \tag{10}$$

Subsequently, the increase in the degradation efficiency of the MB in the presence of the prepared g-C_3N_4/MIL-88B(Fe) nanocomposite can be attributed to the interface formed between g-C_3N_4 and MIL-88B(Fe), which improves the separation of charge carriers. Also, the photo- generated electrons accelerate the Fe(II)/Fe(III) cycle and thus cause the synergistic effect of the photocatalyst and photo-Fenton process [17]. The use of visible light, decrease in band gap energy, and the different contributions of active species $OH^\bullet$, $O_2^{\bullet-}$, h^+ and the presence of H_2O_2 are other reasons for the excellent performance of the process [13, 18].

For comparison between the g-C_3N_4/MIL-88B(Fe) photocatalyst and the photocatalysts prepared in other studies, table 1 is presented. In which, various parameters of photo-Fenton or photocatalytic degradation of different organic pollutants are summerized. The g-C_3N_4/MIL-88B(Fe) photocatalyst has shown a high degradation rate constant of 0.21 min^{-1} under photo-Fenton reaction condition. The results of the present study are comparable to the other studies, done by other researchers.

4. Conclusions

Since it is common to use the photo-Fenton process to remove various pollutants, in this research, nanocomposite of g-C_3N_4 with MIL-88B(Fe), which has iron metal cores, was used to remove MB dye pollutant. The presence of MIL-88B(Fe) and g-C_3N_4 together caused an increase in the separation of charge carriers, an increase in absorption in the visible light region, and finally, an increase in the removal efficiency of MB.

Acknowledgment

It should be noted that Dr. A. Naseri and Prof. A. H. Hamidian are both corresponding authors.
The authors acknowledge the National Elites Foundation and the Agricultural Research, Education and Extension Organization (AREEO) for their financial support.

Table 1. Various photocatalysts prepared in other studies, as well as different parameters of photocatalytic or photo-Fenton reactions to degrade organic pollutants over the photocatalysts.

Photocatalyst	Synthesis method	Photocatalyst weight	Light source	Pollutant	Pollutant concentration (mg/L)	Degradation efficiency (%)	Degradation rate constant (min^{-1})	Time of degradation	Degradation process	Ref.
BF-CM-rod	solvothermal	40 mg	500 W Xe lamp	Rhodamine B	10	95	-	30 min dark + 60 min light	photocatalytic	[19]
g-C_3N_4/NH_2-MIL-88B(Fe)	hydrothermal	50 mg	500W Xe lamp	Methylene Blue	30	100	0.01916	12 h dark + 120 min light	photo-Fenton-like	[20]
U-g-C_3N_4/NH_2-MIL-101(Fe)	solvothermal	-	solar irradiation	2,6-dichlorophen 2,4,5-trichlorophenol	-	98.7 97.3	-	3 h	photo-Fenton-like	[21]
g-C_3N_4/PDI@NH_2-MIL-53(Fe)	hydrothermal	0.4 g/L	5 W LED white lamp	Tetracycline Carbamazepine Bisphenol A P-Nitrophenol	50	90 78 100 100	-	1.5 h dark + (1 h 2.5 h 10 min 30 min) light	photo-Fenton-like	[22]
Fe-POM/CNNS-Nvac	hydrothermal	50 mg	300W Xenon lamp	Tetracycline hydrochloride Atrazine Alachor Tetrachlorophenol Methyl Orange	20 5 10 20 20	96.5 81. 6 91.1 95 100	0.1520 0.0892 0.1312 0.1577 0.1604	30 min dark + 18 min light	photo-Fenton	[23]
g-C_3N_4/MIL-88B(Fe)	solvothermal	10 mg	15 W UV lamp + 50 W LED white lamp	Methylene Blue	5	100	0.21	60 min dark + 20 min light	photo-Fenton	This work

References

1. M A Hassaan, A El Nemr, and A Hassaan, *Am. J. Environ. Sci. Eng*. **1** (2017) 64.
2. E Forgacs, T Cserháti, and G Oros, *Environ. Int.* **30** (2004) 953.
3. M Malakootian and A Dehdari rad, *Rums_Journal.* **14** (2016) 827.
4. F Mohebbi et al., *Int. Arch. Heal. Sci*. **8** (2021) 127.
5. Y Gao et al., *J. Memb. Sci*. **626** (2021) 119192.
6. M N Chong et al., *Water Res.* **44** (2010) 2997.
7. Y Pi et al., *Chem. Eng. J.* **337** (2018) 351.
8. A Naseri et al., *Iran. J. Phys*. Res. **20** (2020) 273.
9. A Naseri et al., *Ceram. Int.* **47** (2021) 26185.
10. X Liao et al., *Appl. Surf. Sci.* **503** (2020) 144089.
11. C Hu et al., *Chem. Eng. J.* **418** (2021) 129469.
12. H He et al., *Chem. Eng. J*. **427** (2022) 131962.
13. S Su et al., *Appl. Surf. Sci*. **537** (2021) 147890.
14. T Guo et al., *Appl. Surf. Sci.* **469** (2019) 331.
15. P Zhou, J Yu, and M Jaroniec, *Adv. Mater.* **26** (2014) 4920.
16. Q Wu et al., *Appl. Catal. B: Environ*. **263** (2020) 118282.
17. Y Ma et al., *J. Alloys Compd*. **870** (2021) 159524.
18. Y Deng et al., *Adv. Funct. Mater*. **30** (2020) 2002353.
19. X Liao et al., *Appl. Surf. Sci.* **503** (2020) 144089.
20. X Li et al., *Appl. Catal. B Environ*. **202** (2017) 653.
21. S Su et al., *Appl. Surf. Sci.* **537** (2021) 147890.
22. Y Li et al., *Appl. Catal. B Environ*. **250** (2019) 150.
23. J Jiang et al., *Appl. Catal. B Environ*. **278** (2020) 119349.